



Influence of spark plasma sintering temperature on porous titanium microstructural integrity, airflow resistance, and space holder removal

Isaac M. Makena¹ · Mxolisi B. Shongwe¹ · Ronald Machaka² · Wallace R. Matizamhuka³

Received: 17 April 2019 / Accepted: 13 June 2019 / Published online: 9 July 2019
© Springer-Verlag London Ltd., part of Springer Nature 2019

Abstract

Porous titanium samples were sintered at four different temperatures (500, 550, 600, and 650 °C), by following the spark plasma sintering (SPS)/space holder (SH) route. The aim was to study the effect of sintering temperature on the structural integrity and space holder (NaCl) removal, as well as airflow resistance. The porous titanium was characterized by X-ray diffraction (XRD) and scanning electron microscopy in conjunction with energy-dispersive X-ray spectroscopy (EDS). SEM images of the porous samples showed an appropriate range of pore sizes above 100 μm and interconnectivity. Fracture surfaces reveal the formation and growth of sintering necks between adjacent particles which becomes clearer with increasing temperature. The EDS and XRD analysis showed that there are no contaminations or inclusions of NaCl in the sintered porous samples. The most efficient leaching parameters, which are adequate to completely remove the space holder, were by immersion in hot water, for at least 5 h (five cycles). An increase in sintering temperature significantly reduces the material porosity level, and consequently increases the airflow resistance through the material.

Keywords Spark plasma sintering · Microstructure · NaCl dissolution · Airflow resistance · Porous titanium

1 Introduction

The loss of structure and functions of the human skeleton is often restored by implanting metallic biomaterials. Joint replacements, implant plates, pins, and rods, dental tooth implants, spinal fusion cages, etc. are highly reported in the field of orthopedics, and this necessitates the research and development of new and improved implants [1, 2]. The target is to find implant materials having elastic modulus as low as that of a human bone (cortical bone around 20–30 GPa). Low

modulus/stiffness implants reduce stress shielding effect and have a consequent increase in the in vivo life span [3]. Metallic biomaterials which are made of titanium (Ti) and its alloys are widely reported as favorites in the market, and this is due to their properties such as low elastic modulus, low density, super biocompatibility, and high strength/density ratio [4–6]. These materials possess the lowest elastic modulus as compared to their counterparts (110 GPa (Ti) and 114 GPa (Ti-6Al-4V), 50% lower than Co-Cr). However, the concern remains as the stiffness of these implants is very high relative to that of a human bone [6]. This elastic modulus mismatch with respect to the bone has been identified by Ridzwan [7] as one of the major reasons for implant loosening and bone resorption (due to stress shielding phenomenon). Manufacturing of implants with lower stiffness property could be a solution. In that sense, the development of porous materials is an alternative approach to achieve a stiffness reduction [4–6]. Additionally, porous materials can provide biological anchorage for the surrounding bone tissue via the ingrowth of mineralized tissue into the pore spaces [8]. This way, the progression of implant loosening can be hindered. Therefore, the architecture of a porous implant needs to be optimized to

✉ Isaac M. Makena
MakenaIM1@tut.ac.za; makenaisaac@yahoo.co.za

¹ Department of Chemical, Metallurgical and Materials Engineering, Tshwane University of Technology (TUT), Pretoria, South Africa

² Light Metals, Materials Science and Manufacturing, Council for Scientific and Industrial Research (CSIR), Pretoria, South Africa

³ Department of Metallurgical Engineering, Vaal University of Technology (VUT), Vanderbijlpark, South Africa

allow for adequate tissue ingrowth. As reported by de Vasconcellos et al. [9], Dabrowski et al. [10], and Loh and Choong [11], the size of the pores must be large enough ($\geq 100 \mu\text{m}$) to allow for bone ingrowth and must be interconnected to maintain the vascular system required for continuing bone development.

Several methods, such as slurry foaming [12], slip casting [13–15], loose powder sintering (Torres et al. 2014) and [16–17], hollow sphere sintering [18], and reactive sintering [19], are widely used to produce porous materials. The use of conventional powder metallurgy (PM) route to produce porous materials is well preferred due to its low operational costs and flexibility [4–6, 19]. However, most of the abovementioned methods provide limited porosity [20, 21]. This then gave rise to the use of space holder technique as it allows the precise control of macroporosity, by controlling the pore shape, size, and distribution with the space holders [22]. Torres et al. [16] compared the properties of loose powder sintered implants with space holder foams and reported that the most suitable stiffness values of the porous Ti samples are obtained by space holder technique, with interconnected pores of appropriate size. Ye et al. [23], Torres et al. [24], and Jha et al. [25], among other researchers, reported the advantages of using NaCl as a space holder material. The preference of NaCl is due to its high

melting point (801°C) and mechanical strength; hence, it can withstand high sintering temperatures and hot-pressing procedure without evaporation or decomposition, which are typically the problems of other space holder materials [23]. The work of Patnaik [26] reports that NaCl as the space holder is associated with low costs, lower toxicity from residual content, and reduced etching of metal during dissolution, as well as fast dissolution in water. Lower toxic space holders are extremely recommended since these materials are used as implants, and it is difficult at times to ensure that the entire spacer holder is removed from the foam [27]. Therefore, the application of NaCl as a space holder material requires that NaCl is entirely removed before being put in service. It is well known that residual NaCl particles (when the NaCl particles are present isolated in the matrix and do not get in contact with water) can cause corrosion of the metal matrix because of the incomplete dissolution in some pores [28].

In this work, titanium metal powder was consolidated by SPS at four different sintering temperatures, i.e., 500, 550, 600, and 650°C . To obtain a porous sample, NaCl particles were used as space holders. The effect of sintering temperature on structural integrity, NaCl removal, and airflow resistance was studied. The microstructure was characterized using SEM in conjunction with EDS. For phase analysis, XRD was used.

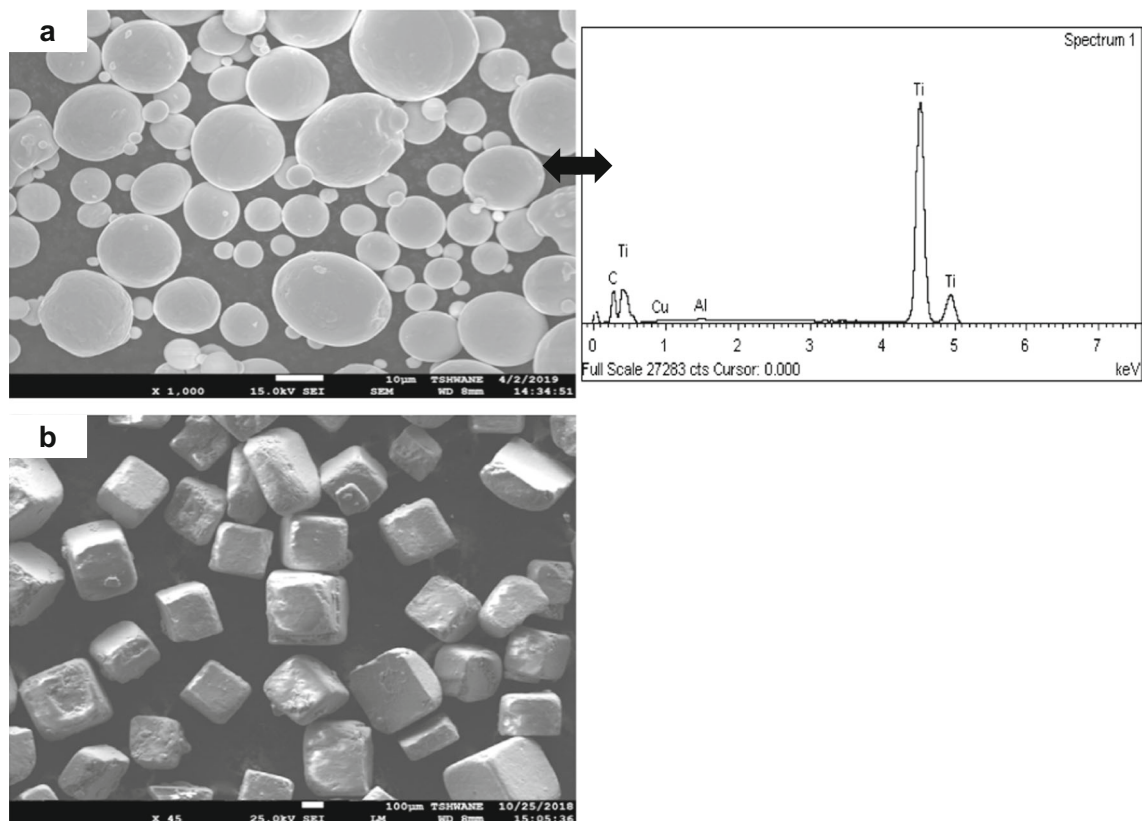


Fig. 1 SEM images of the a cp-Ti powder with EDS, and b NaCl

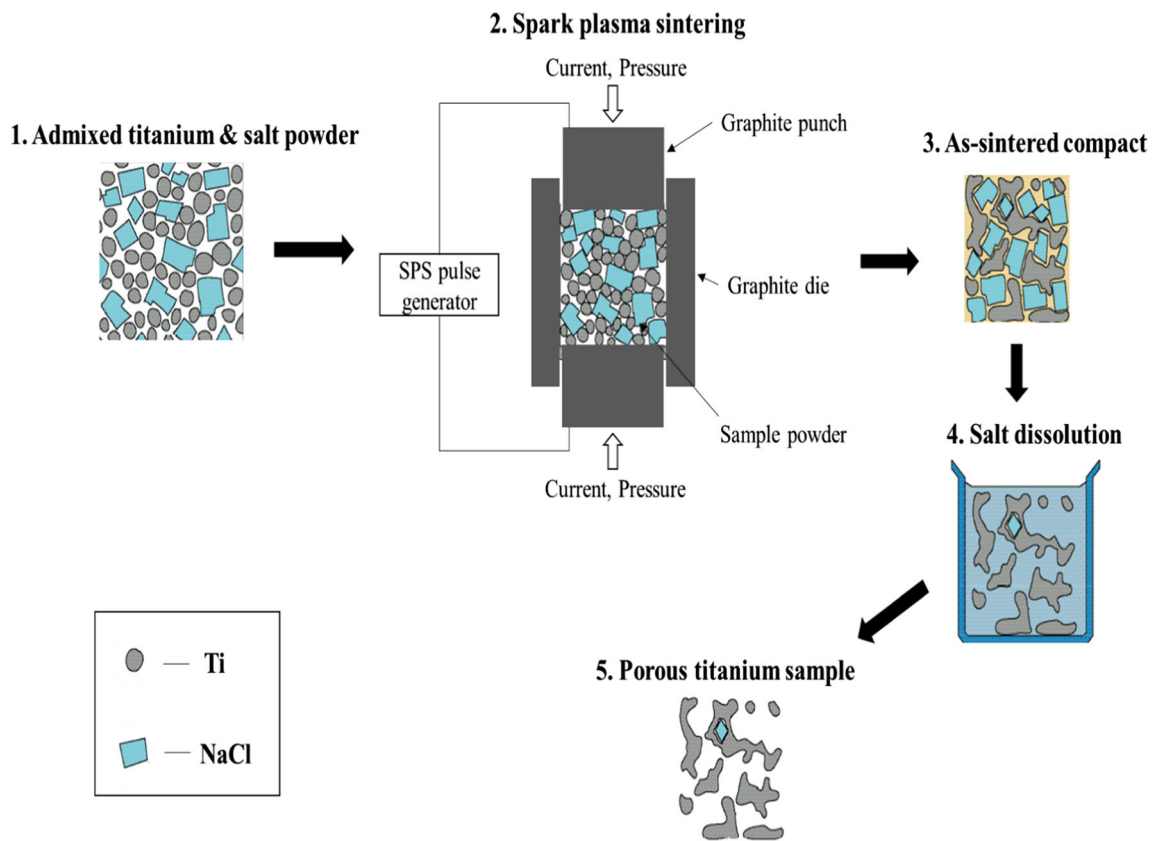


Fig. 2 Production of an open-cell titanium foam by sintering admixed titanium metal powder and NaCl [4]

2 Experimental procedure

2.1 Materials and specimen preparation by SPS/SH

In this work, the elemental titanium (Ti) metal powder (grade 1, $\leq 25 \mu\text{m}$, TLS Technik GMBH & Co., Germany) was blended with 99.0% pure NaCl particles ($212 \mu\text{m} \geq \text{size} \leq 425 \mu\text{m}$) and polyethylene glycol (PEG-400, binder). As shown in Fig. 1a, b, the commercially pure Ti (cp-Ti) metal powder particles used in this study are spherical with smooth surfaces, while NaCl granules have a cubic shape with round angles. The EDS of Ti powder confirms Ti as a dominating constituent with minor traces of carbon (C), copper (Cu), and aluminum (Al) elements. Porous Ti foams

were produced by mixing and compacting metal powders with a NaCl space holder which is later removed after sintering, by dissolution to leave pores. A schematic diagram summarizing the flow of the whole fabricating process is shown in Fig. 2, with steps 1 up to 5. The process shows the possibilities of having traces of NaCl space holder particles being trapped inside closed pores.

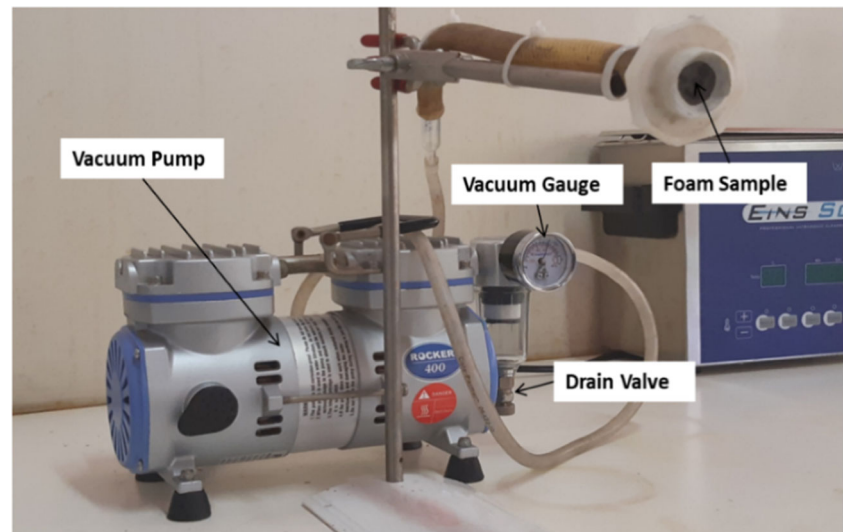
The weighed powders were blended using a Turbula mixer at a rotational speed of 49 rpm (moderate rotating speed to minimize impact energy and thus fewer chances of particle deformations) for 3 h to ensure uniform distribution of the mixture constituents.

Figure 2, steps 1–3 The admixed mixture was then poured into cylindrical graphite die having an internal diameter of 20 mm and sintered using the spark plasma sintering system (HPD5, FCT Systeme GmbH, Germany). Graphite paper is normally put in between the die and mixture (sample) to avoid direct contact of the powder with die and for easy removal of the sample after sintering. The sintering temperature is measured by an optical pyrometer which is implanted in the SPS apparatus at 3 mm from the top of the sample surface. Discs of 20-mm diameter and of approximately 8 mm in height were targeted. The powders were subjected to different sintering temperatures

Table 1 Optimization of NaCl dissolution/removal rate

Dissolution water Temp. (°C)	Duration per cycle
26	1 hour
45	
55	
65	
75	

Fig. 3 Picture of an experimental setup



(500, 550, 600, and 650 °C), with fixed holding time and pressure of 10 min and 50 MPa, respectively. The maximum temperature was reached at a constant rate of 50 °C/min for all the samples. At the end of the prescribed holding time, the applied current automatically switches off and the specimen rapidly cools to room temperature.

Figure 2, steps 4–5 Porous foams were then obtained through the dissolution of NaCl space holder in renewed deionized water at different temperatures shown in Table 1. Distilled water is changed after every cycle of testing (i.e., 1 h). After each cycle, the sample is dried in a vacuum drier (200 mbar vacuum, 100 °C temp.) for 2/3 h and then weighed to compare

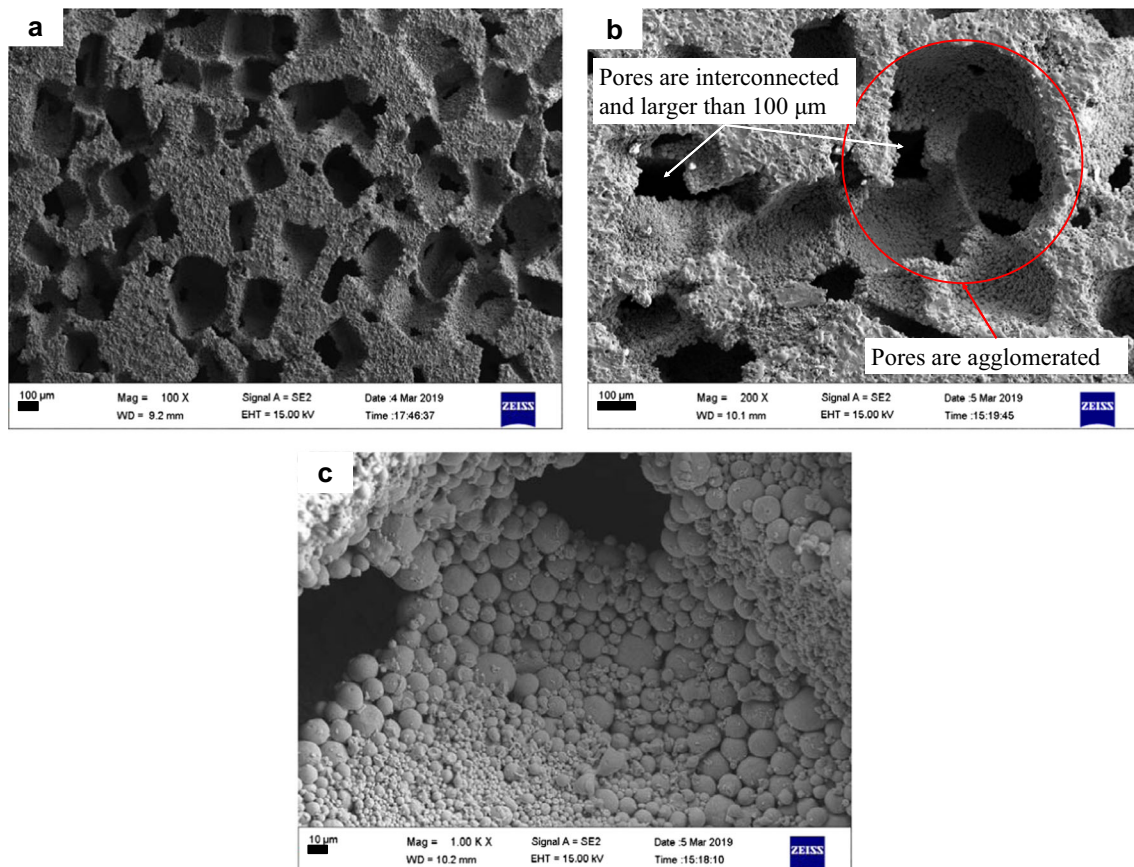


Fig. 4 SEM micrograph of porous Ti sintered at 650 °C showing **a** cross-section of homogeneous foam, **b** enlarged view of pore morphology, and **c** inside view of a pore

it with the weight of the initial (Ti + NaCl) sample mass to get the relative mass percentage.

2.2 Material characterization

Microstructural characterization was performed by scanning electron microscope (Carl Zeiss SEM) in conjunction with EDS, and the imaging was conducted on the cross-section of the sample. For phase analysis, XRD was used. The porosity (p) of the porous Ti, denoting the ratio of the pore volume to the total volume, was calculated using the formula:

$$p = (1 - \rho / \rho_s) \times 100\%$$

where ρ and ρ_s represent the apparent density of the sintered porous Ti and the theoretical density of solid Ti, respectively; ρ / ρ_s is the relative density. The apparent density of the porous Ti was determined from its weight and dimensional measurements; that is, using a Vernier caliper or ruler, length, depth, and width of the sample in centimeters can be measured. Airflow resistance experiments were performed in a small open-loop tunnel as shown in a picture in Fig. 3. Room air was drawn into the tunnel by a suction vacuum pump located

at the exit, which had a drain valve for controlling the volumetric flow rate. A 9-mm diameter pipe was used as a tunnel. The diameter size of the tunnel's test section was 15 mm. Each sample measured 8.0 mm in the flow direction and had a cross-sectional area of 314 mm². The sides of each foam sample that constituted its outer perimeter were covered with a thin Bostik adhesive, and the sample was placed in the tunnel's test section. The remaining two sides were kept open to the airflow. The Bostik ensured that the flow would travel through the foam only, allowing a negligible flow between the foam and the tunnel's walls. For the airflow resistance, the steady-state unidirectional static airflow was measured using vacuum gauge located at 3.5 cm just after the pump.

3 Results and discussion

3.1 Microstructure

The SEM micrographs of the porous Ti sintered with the temperature of 650 °C are shown in Fig. 4. The SEM images show that the porosities are homogeneously dispersed (Fig. 4a). These pores were created due to leaching out of NaCl space

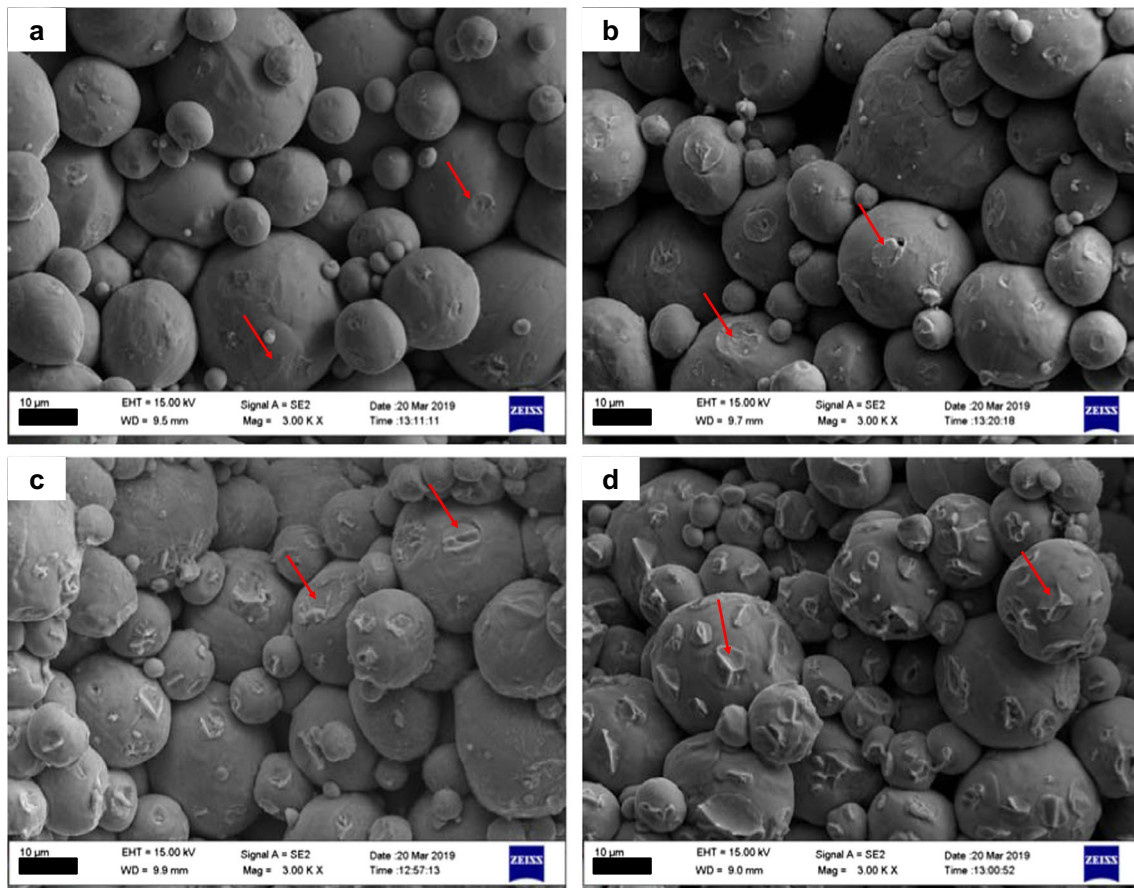


Fig. 5 SEM images of fracture surface (the red arrows indicate sintering necks) of the porous Ti foams sintered at different temperatures **a** 500 °C, **b** 550 °C, **c** 600 °C, and **d** 650 °C

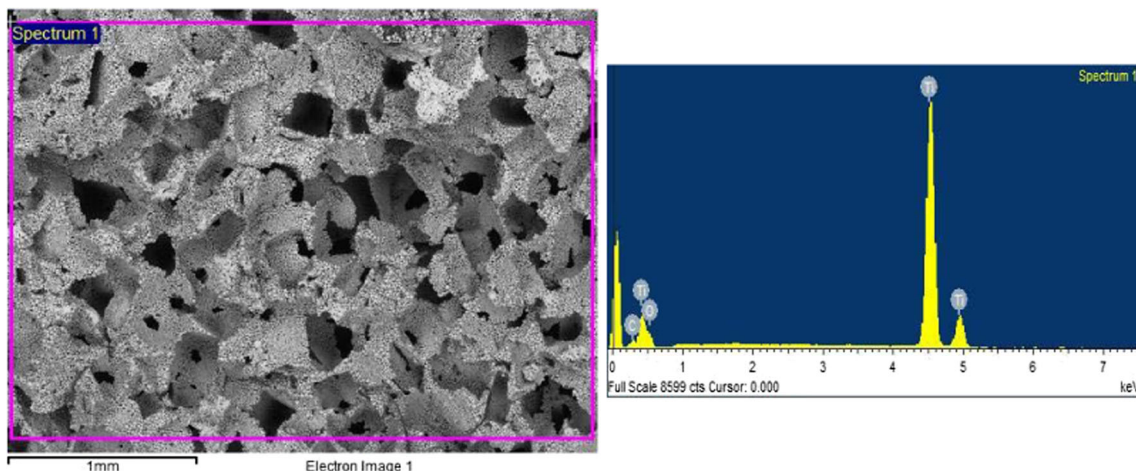


Fig. 6 Typical EDS spectrum of the porous Ti scaffold sintered at 650 °C

holder. Looking at Fig. 4b, it was observed that the pores are open and interconnected forming a three-dimensional, nonhomogeneous network with high porosity. Furthermore, the pore size of the porous Ti after the removal of NaCl meets the preliminary requirement for porous implant scaffolds as a mean pore size larger than 100 μm can allow bone tissue ingrowth [29, 30]. In addition, agglomeration of pores is noted in some regions (see the red circle); and this increases the overall mean pore size. Finally, Ti particles were still visible after sintering at the temperature of 650 °C (Fig. 4c). Figure 5 shows the fracture surface morphologies of the sintered porous Ti foams sintered at four different temperatures. The sintered necks have successfully formed between titanium particles (see red arrows). This shows that the sintering process had adequate parameters

to assure bonding between Ti particles. The so-called sintering necks become more apparent in number and size when the sintering temperature is increased from 500 to 650 °C. This can be attributed to the facilitated thermodynamic atomic diffusions which occur at higher temperatures, leading to easier neck formation and growth between adjacent particles. Ductile rupture mode is clearly visible at the sintering temperature of 650 °C.

Additionally, to SEM investigation, the chemical composition of porous titanium was determined by EDS analysis. As presented in Fig. 6, titanium (Ti) is identified as a main chemical element in the investigated sintered samples. The presence of oxygen (O) and a minor amount of carbon (C) are also detected with no trace of sodium (Na) and chlorine (Cl). This confirms that NaCl is completely leached out from Ti foam by hot water when the sintered foams are treated in a hot water bath. The presence of oxygen is believed to be due to the oxidation of Ti (to form TiO_2) with the residual air within the sample before sintering or with the gases of PEG-400 binder ($\text{C}_{2n}\text{H}_{4n} + 2\text{O}_{n+1}$). The detected carbon can either be traced to be introduced either with the as-received Ti powder or also as a contaminant from the binder gases. Given the high vacuum in the sintering chamber and the low boiling point of the PEG-400 (~ 250 °C), it is assumed that the binder can decompose into gases which escape from the admixed compact during early stages of sintering. To corroborate these results, XRD analysis was conducted to identify the phases present in the starting and sintered materials. The XRD patterns shown in Fig. 7 are related to the raw NaCl, cp-Ti powder, and sintered porous Ti samples (sintered at 500 and 650 °C, each). Comparing the diffraction peaks of the powders and sintered samples, it was found that the sintered samples had the same peak shape as that of the original Ti powder, indicating that the powder was not contaminated during and after sintering. However, the peaks for the sintered porous Ti samples are extremely shorter compared to the peaks of both NaCl and Ti metal powder. This is because the difference of sample

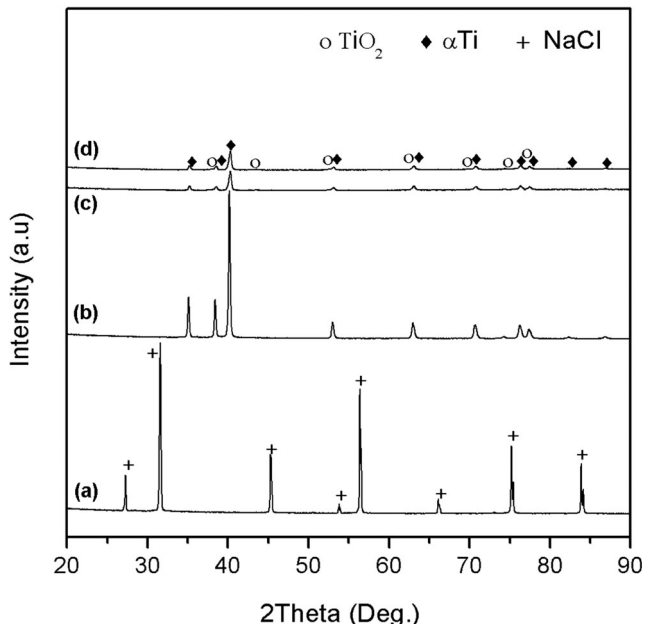


Fig. 7 X-ray diffraction of **a** NaCl, **b** raw Ti powder, **c** porous Ti sintered at 500 °C, and **d** porous Ti sintered at 650 °C

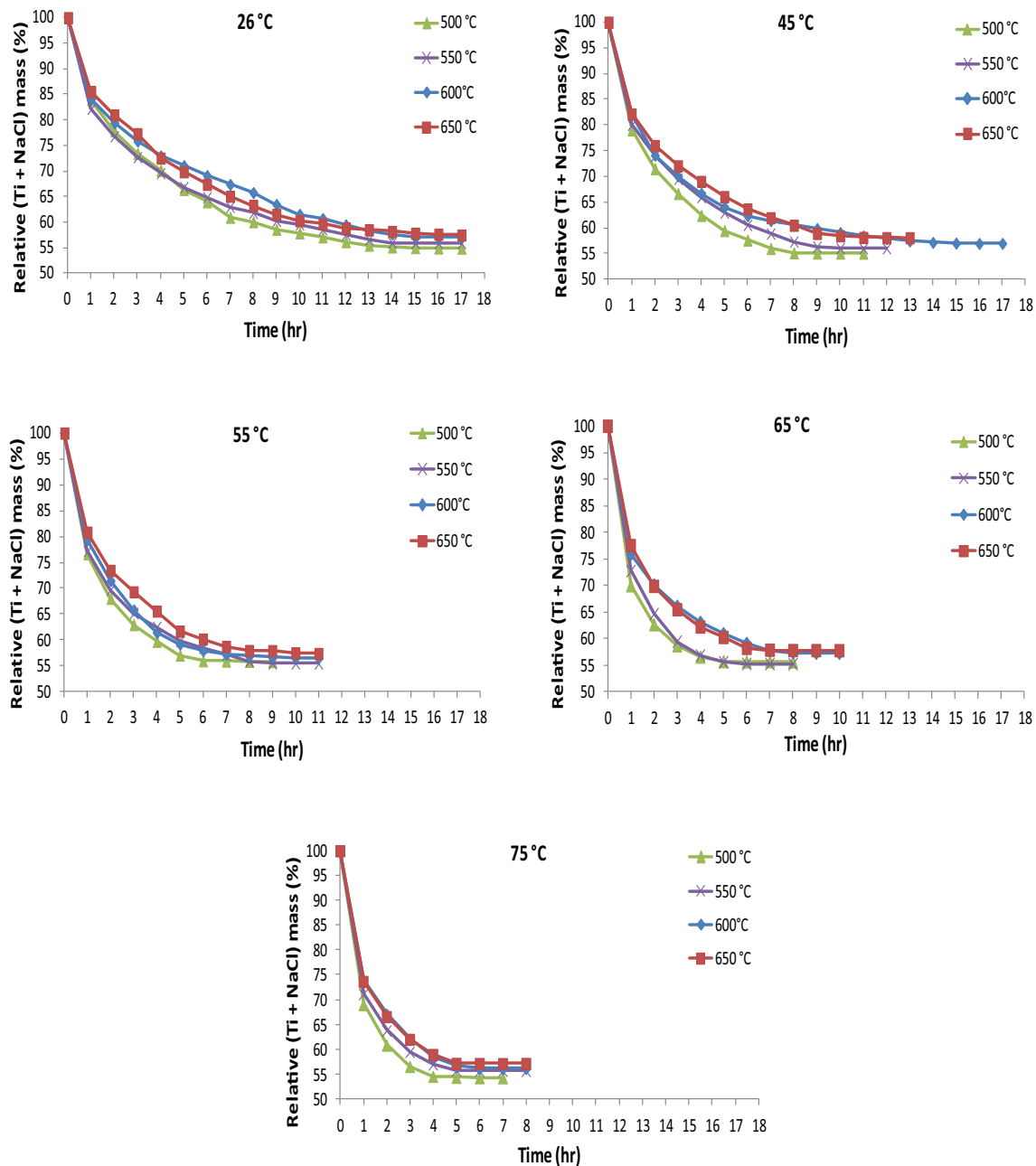


Fig. 8 Dissolution rate of samples, for different dissolution water temperatures, sintered at 500, 550, 600, and 650 °C

morphology in sintered porous form has lowered the intensity of diffraction patterns compared to the sample morphology in the form of powder. The surface of the powder sample was prepared to be uniform and smooth. In contrast, the surface of the porous sintered sample was rough and porous which cause some of the X-rays to be diffracted away from the sensor [31]. Therefore, this results in the peaks of sintered porous samples appearing shorter than the ones for powders. No significant differences in the patterns with increasing sintering temperature were noted. The patterns reveal only the peaks corresponding to that of α Ti and titanium oxide (TiO_2). It is thus confirmed that porous Ti foams

does not contain NaCl and any other phases such as titanium chloride.

3.2 NaCl dissolution

Figures 8, 9, and 10 present the effects of two parameters on the rate of NaCl dissolution: sintering temperature (500, 550, 600, and 650 °C), and dissolution water temperature (26, 45, 55, 65, and 75 °C). The general trend of the curves is observed (Figs. 8 and 9); samples sintered with the lowest temperature (500 °C) required the shortest time for complete NaCl

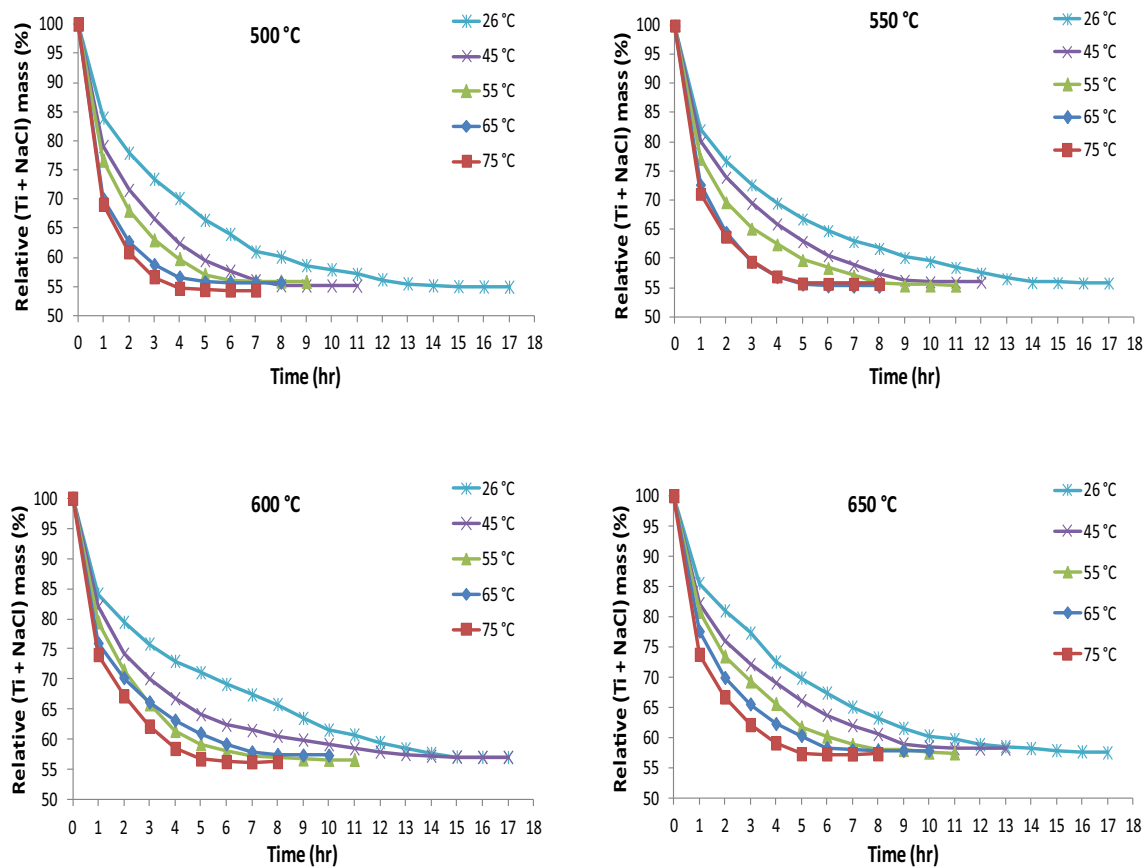


Fig. 9 Dissolution rate of sample, sintered at 500, 550, 600, and 650 °C, for different dissolution water temperatures

dissolution (Fig. 10). This behavior is the logical consequence of the higher porosities associated with lower sintering temperatures (Fig. 11). For all dissolution curves, the slope of the weight loss shows that the initial Ti mass is reached; the assumptions are made from the point that further application of additional cycles gives constant (Ti + NaCl) mass, suggesting that all the NaCl initially in the sample has been dissolved into the water. However, despite the obtained values suggesting total elimination of NaCl without any loss of Ti, some

conditions did not achieve this (Fig. 8, samples sintered at the temperature of 650 °C shows relatively low (Ti + NaCl) mass reduction). This can be due to the presence of residual NaCl trapped within the closed pores or the loss of NaCl during sintering. As reported by Kaufmann [32] and Akella et al. [33], the NaCl can easily get fused during heating (at temperatures lower than its actual melting point when in high vacuum conditions) and then evaporate. Thus, the samples sintered at higher temperatures are prone to lose slightly

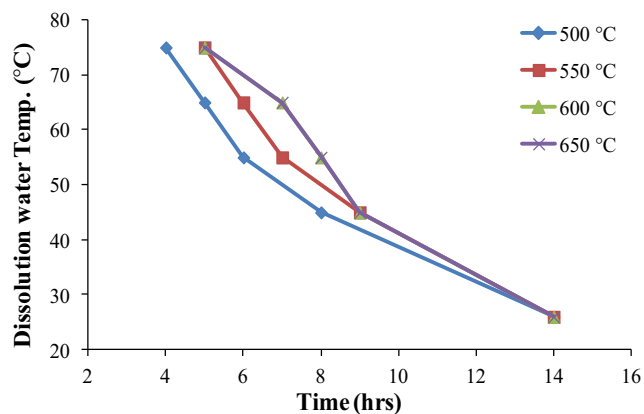


Fig. 10 Time to reach constant (Ti + NaCl) mass as a function of dissolution temperature

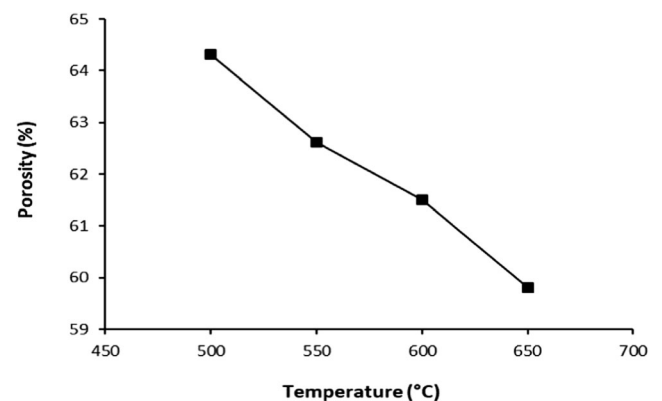


Fig. 11 Porosity (ϵ) of sintered porous titanium as a function of sintering temperature

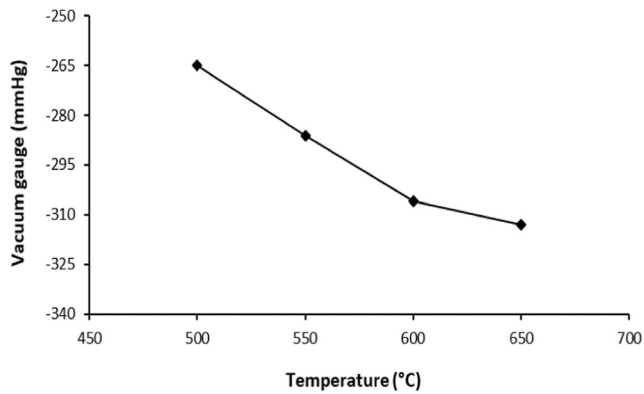


Fig. 12 Vacuum gauge reading as a function of sintering temperature

higher NaCl mass during sintering as compared to the ones sintered at 500 °C. As seen from the SEM micrographs and EDS analysis, there was no sign or detection of NaCl in the sample, making the former suggestion of trapped NaCl less considerable. The samples sintered at a temperature of 500 °C shows the highest relative (Ti + NaCl) mass loss (Fig. 8). From the practical point of view (also the lack of neck formation between adjacent particles), the samples sintered at the temperature of 500 °C involved a risk of sample collapse or even Ti losses; both of which are associated with sample handling and this might have been the reason for the high relative (Ti + NaCl) mass loss obtained with this temperature.

In Fig. 9, the dissolution rate substantially increases with water temperature. This can be related to the molecular thermodynamic movement which increases with temperature; that is, the kinetic energies of the molecules in the solid salt and liquid water are accelerated [34]. Subsequently, the dissolution rate of solid NaCl becomes faster. There is no significant difference noted between the slopes of room temperature dissolution rates for all the sintering temperatures. From Fig. 10, it is observed that the effect of dissolution temperature is dominant when the temperature is 45 °C or above. It takes approximately 14 h (14 cycles) to reach a constant (Ti + NaCl) mass when dissolution is performed at room temperature. The application of high temperatures for NaCl dissolution drastically reduced these hours/cycles to less than 5 h/cycles. Furthermore, a constant mass for 500 °C sintered samples was reached after 4 cycles which are 1 cycle less, compared to other samples sintered at 550, 600, and 650 °C.

3.3 Porosity measurements

Highly porous materials allow the bone to grow into the implant and thus improve the fixation and stability and the remodeling between the implant and the human tissue. This can be related to the fact that transportation of body fluids is facilitated as porosity level increases, because adequate space for cell adhesion is provided [35, 36]. The effect of sintering

temperature on the porosity (ϵ) level of porous Ti is shown in Fig. 11. Increasing sintering temperature from 500 to 650 °C decreases the sample porosity level. This was expected, since at higher sintering temperatures metal powder particles are reported to be becoming soft and ductile, giving rise to an increase in the contact areas and a slight decrease in the void size [37]. The highest porosity level as high as $64.32 \pm 0.94\%$ was reported with the sintering temperature of 500 °C. Thereafter, an increase in sintering temperature to 550, 600, and 650 °C significantly reduces the porosity level.

3.4 Pressure drops

Figure 12 shows the comparison of the pressure drop for the four foams sintered at different temperatures. Plotting such data can help predict the effect of sintering temperature on the interconnectivity/permeability of the open pores. Herein, materials with high porosity (open pores) are expected to display a low-pressure drop. Generally, pore characteristics, such as interconnectivity, morphology, size, and surface texture, are playing a major role in airflow resistance. As shown, the measured pressure drop is observed to be increasing with sintering temperature. The foam sintered at the temperature of 500 °C produces the lowermost pressure drop as compared to the 550, 600, and 650 °C sintered foams. This can be primarily attributed to the high level of open porosities reported earlier for the Ti samples sintered at the temperature of 500 °C [10]. We can thus safely say the significant increase of the permeability is observed with an increase of the total and open porosity of titanium samples.

4 Conclusions

Porous titanium was fabricated by spark plasma sintering with NaCl as a space holder. The effect of sintering temperature on the structural integrity, NaCl removal, and resistance to airflow was studied and the following conclusions were made:

- 1) Sintering necks became more apparent in number and sizes when the sintering temperature was increased from 500 to 650 °C. There was no sign or detection of NaCl surpluses left in the samples after the dissolution tests.
- 2) Samples sintered at the temperature of 500 °C (the lowest sintering temperature) required the shortest time to remove the salt. An increase in dissolution water temperature from room temperature (26 °C) to higher temperatures (65–75°) reduced the duration needed for NaCl space holder removal from 14 h to less than 5 h.
- 3) An increase in sintering temperature also reduced the level of total porosity of porous Ti foams, and consequently, the resistance to airflow was increased.

Future work is needed on studying the effect of sintering temperature on the compressive strength of titanium foams. Also, it is necessary to evaluate the effect of various porosities and pore size distributions on the foam's static and cyclic compressive strength, and cytocompatibility. This work is part of a comprehensive work which aims to develop porous beta-titanium alloy foams for biomaterial applications.

Acknowledgments This work is based on the research supported in part by the National Research Foundation of South Africa for the grant, Unique Grant No. 113838. Research facilities were supported by the Institute for NanoEngineering Research, Tshwane University of Technology.

Funding information This study received financial assistance from the Department of Higher Education and Training (DHET) funding under the Tshwane University of Technology, Emerging Program Grant.

References

- Kremers HM, Larson DR, Crowson CS, Kremers WK, Washington RE, Steiner CA, Jiranek WA, Berry DJ (2015) Prevalence of total hip and knee replacement in the United States. *J Bone Joint Surg, Incorporated* 97(13):86–97
- Aherwar A, Singh AK, Patnaik A (2016) Current and future biocompatibility aspects of biomaterials for hip prosthesis. *AIMS Bioeng* 3(1):23–43
- Bandyopadhyay A, Espana F, Balla VK, Bose S, Ohgami Y, Davies NM (2010) Influence of porosity on mechanical properties and the in-vivo response of Ti6Al4V implants. *Acta Biomater* 6(4):1640–1648
- Kennedy A (2012) Porous metals and metal foams made from powders. *Powder Metallurgy*. In: Katsuyoshi Kondoh (ed) ISBN: 978-953-51-0071-3, InTech
- Li Y, Yang C, Zhao H, Qu S, Li X, Li Y (2014) New developments of Ti-based alloys for biomedical applications. *Materials* 7:1709–1800
- Babaie E, Bhaduri SB (2018) Fabrication aspects of porous biomaterials in orthopedic applications: A Review. *ACS Biomater Sci Eng* 4:1–39
- Ridzwan MIZ, Shuib S, Hassan AY, Shokri AA, Mohamad Ibrahim MN (2007) Problem of stress shielding and improvement to the hip implant designs: An in vivo histological study. *PLoS ONE* 13(10):e0206228
- Chimutengwende-Gordon M, Dowling R, Pendegrass C, Blunn G (2018) Determining the porous structure for optimal soft-tissue ingrowth: an in vivo histological study. *PLoS ONE* 13(10):206–228
- de Vasconcellos LMR, Leite DO, de Oliveira FN, Carvalho YR, Cairo CAA (2010) Evaluation of bone ingrowth into porous titanium implant: histomorphometric analysis in rabbits. *Braz Oral Res* 24(4):399–405
- Dabrowski B, Kaminski J, Swieszkowski W, Kurzydowski KJ (2011) Porous titanium scaffolds for biomedical applications: corrosion resistance and structure investigation. *Mater Sci Forum* 674:41–46
- Loh QL, Choong C (2013) Three-dimensional scaffolds for tissue engineering applications: role of porosity and pore size. *Tissue Eng B* 19:Number 6
- Ahmad S, Muhamad N, Mughtar A, Sahari J, Jamaludin KR, Ibrahim MHI, Mohamad Nor NH, Murtadhahadi I (2008) Producing of titanium foam using titanium alloy (Al₃Ti) by slurry method, Brunei Int. Conf. of Eng. and Techn. (BICET) 34.11.2008 Brunei
- Neirinck B, Matthews T, Braem A, Fransaeer J, Van der Biest O, Vleugels J (2009) Preparation of titanium foams by slip casting of particle stabilized emulsions. *Adv Eng Mater* 11(8):633–636
- Yan L, Wu J, Zhang L, Liu X, Zhou K, Su B (2017) Pore structures and mechanical properties of porous titanium scaffolds by bidirectional freeze casting. *Mater Sci Eng C* 75:335–340
- Yook SW, Kim HE, Koh YH (2009) Fabrication of porous titanium scaffolds with high compressive strength using camphene-based freeze casting. *Mater Lett* 63:1502–1504
- Torres Y, Lascano S, Bris J, Pavón J, Rodríguez JA (2014) Development of porous titanium for biomedical applications: A comparison between loose sintering and space-holder techniques. *Mater Sci Eng C*, 37:148–155
- Esen Z, Bor ET, Bor S (2009) Characterization of loose powder sintered porous titanium and Ti6Al4V alloy. *Turk J Eng Environ Sci* 33:207–219
- Szyniszewski ST, Smith BH, Hajjar JF, Schafer BW, Arwade SR (2014) The mechanical properties and modeling of a sintered hollow sphere steel foam. *Mater Des* 54:1083–1094
- Novák P, Salvetr P, Školáková A, Karlík M, Kopeček J (2017) Effect of alloying elements on the reactive sintering behavior of NiTi alloy. *Mater Sci Forum* 891:447–451
- James WB (2015) Powder metallurgy methods and applications. *Powder Metall. ASM Handb* 7:9–19
- Sharma B, Vajpai SK, Ameyama K (2018) An efficient powder metallurgy processing route to prepare high-performance β Ti-Nb alloys using pure titanium and titanium hydride powders. *Metals* 8(516):1–16
- Xiang C, Zhang Y, Li Z, Zhang H, Huang Y, Tang H (2012) Preparation and compressive behavior of porous titanium prepared by space-holder sintering process. *Proc Ineering* 27:768–774
- Ye B, Dunand DC (2010) Titanium foams produced by solid-state replication of NaCl powders. *Mater Sci Eng A* 528:691–697
- Torres Y, Pavón JJ, Rodríguez JA (2012) Processing and characterization of porous titanium for implants by using NaCl as space holder. *J Mater Process Technol* 212:1061–1069
- Jha N, Mondal DP, Majumdar JD, Badkul A, Jha AK, Khare AK (2013) Highly porous open cell Ti-foam using NaCl as temporary space holder through powder metallurgy route. *Mater Des* 47:810–819
- Patnaik P (2003) Handbook of inorganic chemicals. McGraw-Hill, New York
- Bansiddhi A, Dunand DC (2008) Shape-memory NiTi foams produced by replication of NaCl space-holders. *Acta Biomater* 4:1996–2007
- Prashanth KG, Zhuravleva K, Okulov I, Calin M, Eckert J, Gebert A (2016) Mechanical and corrosion behavior of new generation Ti-45Nb porous alloys implant devices. *Technologies* 4(33):1–12
- Dabrowski B, Swieszkowski W, Godlinski D, Kurzydowski KJ (2010) Highly porous titanium scaffolds for orthopedic applications. *J Biomed Mater Res B Appl Biomater* 95B(1):53–61
- Wang X, Li J, Hu R, Kou H, Zhou L (2013) Mechanical properties of porous titanium with different distributions of pore size. *Trans Nonferrous Metals Soc China* 23:2317–2322
- Jamaludin MI, Kasim NAA, Mohamad Nor NH, Ismail MH (2015) Development of porous Ti-6Al-4V mix with palm stearin binder by metal injection molding technique. *Am J Appl Sci* 12(10):742–751
- Kaufmann DW (1960) Sodium Chloride; the production and properties of salt and brine. Reinhold Pub. Corp., New York

33. Akella J, Vaidya SN, Kennedyn GC (1969) Melting of sodium chloride at pressures to 65 kbar. *Phys Rev B* 2(185):1135–1140
34. Song J, Shi P, Wang Y, Jiang M (2018) Kinetics study on the effect of NaCl on the CaSO₄ dissolution behavior. *IOP Conf Ser: Mater Sci Eng* 301:012154
35. Rosa AL, Crippa GE, Oliveira PT, Taba MJ, Lefebvre LP, Beloti MM (2009) Human alveolar bone cell proliferation, expression of osteoblastic phenotype, and matrix mineralization on porous titanium produced by powder metallurgy. *Clin Oral Implants Res* 20: 472–481
36. Zhang YP, Li DS, Zhang XP (2007) Gradient porosity and large pore size NiTi shape memory alloys. *Scr Mater* 57:1020–1023
37. Öztürk B, Cora ÖN, Koç M (2011) Effect of sintering temperature on the porosity and microhardness of the micro-scale 3-D porous gradient surfaces. In: *Proceedings of the 8th International Conference on Multi-Material Micro Manufacture (4 M)*. pp 176–179

Publisher's note Springer Nature remains neutral with regard to jurisdictional claims in published maps and institutional affiliations.